

**PREPARATION OF V₂O₅ @MESOPOROUS SILICA
SPHERE FOR NOVEL DUAL OXIDATIVE-
ADSORPTIVE DESULFURIZATION**

**Shorouk Shawky*¹ ; Nasser H. Shalaby¹ ; Dalia R. Abd El-Hafiz¹ ;
S. Said¹ ; Maher Helmy Helal² and Sahar K. Mohamed²**

¹ Catalysis lab., Refining department, Egyptian Petroleum Research Institute, Nasr City,
Cairo 11727, Egypt

²Chemistry Department, Faculty of Science, Helwan University, Ain Helwan, Cairo,
11795, Egypt

Key Words: Oxidative-Adsorptive desulfurization; Mesoporous silica
spheres; micelle-template; Vandia.

ABSTRACT:

V₂O₅ nanoparticles were supported on mesoporous silica spheres (V₂O₅/MSS) by impregnation technique. Where mesoporous silica sphere (MSS) was synthesized via micelle-template method. The structure and morphology were tested using XRD, FTIR, BET surface area, TEM, and DLS techniques. The results demonstrated that the samples were amorphous with a mesoporous structure, special interior spaces, and high specific surface area. The prepared sample was tested for dual oxidative/adsorptive performance of model diesel fuel. The desulfurization process was tested in the presence of H₂O₂ as an oxidizing agent at different reaction conditions (temperature, contact time, and initial concentration) using a batch system by either stirring or ultrasonic. The data indicate that V₂O₅/MSS shows good performance toward dual oxidative/adsorptive desulfurization with 100% removal efficiency under sonication within 1.5h but in stirring within 2h at 60°C using 600 ppm initial concentration.

1. INTRODUCTION

Mesoporous materials represent a range of porous materials with 2–50 nm diameters. They are commonly used in numerous fields, catalysis, biomedicine, and sensor. Because of their incredible properties and characteristics, including ultra-high surface areas, controllable pore sizes, and large volumes of pores (1). Various techniques such as Sol-Gel processing(2), Template assisted techniques(3), Microwave-assisted techniques(4), Chemical etching techniques can be used to synthesize mesoporous materials(5). Mesoporous silica are considered a good selection because of their amorphous character and the easy process of sphere formation (6–11).

Moreover, it is known that the earth's crust is rich in the element of vanadium (V), and the vanadium oxides have different forms of crystalline and

*Corresponding author: *Shorouk Shawky*¹

Email: Shorouk.shawky92@gmail.com

Fax: +20 222747433

multi-oxidation state (II – V). Vanadium oxides exhibit significant interactions with molecular or ionic species, higher catalytic efficiency and/or effective correlations between electron and electron (12). From the practical and economical points of view, V_2O_5 has a greater potential to be applied as catalyst active phase for oxidative desulfurization (ODS) process (13). Due to their large pore size with controlled distribution, which may be beneficial in allowing accessibility of large molecular size sulfones to the surface active sites, much attention was paid to development of mesoporous oxide-based materials (14).

On the other hand, the worldwide attention has been drawn to the sulfur content of diesel fuel as after combustion, the sulfur compounds in the fuel are converted to sulfur oxides (SO_x), which cause acid rain and air pollution, as well as catalyst toxicity. Governments worldwide have noticed these concerns and have imposed new strict environmental regulations on fuel sulfur levels to minimize SO_x emissions (15,16). Several approaches have been investigated to remove those heterocyclic sulfur compounds (14,17–22). The traditional fuel sulfur removal method is called hydrodesulfurization (HDS), a well-known catalytic process in the refining industry. However, HDS is not efficient in removing heterocyclic sulfur compounds such as dibenzothiophene (DBT) and its derivatives. It is also demands strict operating conditions such as high temperatures, high pressure, and high consumption of hydrogen(23). Oxidative desulfurization (ODS) is a great alternative approach to hydrodesulfurization. This eliminates the use of costly hydrogen and can be performed under mild conditions with short time of reaction, greater selectivity and efficiency (24,25). In the ODS process, these refractory aromatic organosulfur compounds (such as DBT and its derivatives) are quickly oxidized into their corresponding sulfoxides and highly polar sulfones, which can be removed from the fuel by adsorption or extraction (26). Since heterocyclic sulfur compounds are relatively large molecules, the pore diameter and surface area of the catalyst have to be taken as part of the catalyst design(13). Adsorption desulfurization technology is considered promising alternative method for deep desulfurization, owing to the potential benefits of low capital, the mild operating conditions of temperature and pressure, low environmental impact and greater reaction specificities, and availability of adsorbents with high adsorption capacity (24). The combination of oxidation and adsorption is better than direct adsorption to achieve a better desulfurization performance (27). However, there are few studies reported that consider insitu oxidative-adsorptive desulfurization as a more efficient than either oxidation or adsorption (28–30). In this case, the desulfurization efficiency is generally based on the catalyst/adsorbent system characteristics (31,32).

According to the previous statement, our aim to prepare ordered mesoporous materials with narrow pore size distribution for removal of sulfur compounds from model diesel fuel. Firstly, the mesoporous silica spheres (MSS) will synthesized via micelle-template method then will impregnated with

V₂O₅ using a wet impregnation technique to deposit V₂O₅ on mesoporous silica spheres. The prepared catalyst will be characterized by XRD, FTIR, BET, TEM and DLS techniques. The efficiency of the prepared sample as a catalyst-adsorbent system will be examined for oxidative-adsorptive desulfurization of dibenzothiophene (DBT), as a model diesel oil of sulfur-containing compound, in presence of H₂O₂ as oxidant. To achieve the best selectivity and activity, different factors were studied such as contact time, reaction temperature, and initial concentration of DBT. Additionally, the effect of ultra-sonication versus stirring will be also studied.

2. EXPERIMENTAL:

2.1. Materials:

Tetraethoxysilane (TEOS, 99.9%, Sigma Aldrich), Aqueous ammonia solution (25–28 wt.%, Merck), Ammonium metavanadate (NH₄VO₃, 99.8%, Sigma Aldrich), Cetyltrimethylammonium bromide (CTAB, Sigma Aldrich), Ethanol (EtOH (99 %, Merck Chemicals), Oxalic acid (99.5%, Merck), Dibenzothiophene (99 %, Merck), Hydrogen peroxide (aqueous solution, 30%), Hexane and Deionized water.

2.1.1. Synthesis of mesoporous silica spheres (MSS):

Mesoporous silica sphere (MSS) was prepared via the hydrolysis and condensation of TEOS in an aqueous basic-ethanol medium. Typically, 0.16g of CTAB was dissolved in 100 mL of mixed aqueous solution of ethanol and water with continuous stirring. Then 1.0 mL of TEOS and 1.0 mL of ammonia were added sequentially. The resulting mixture was further stirred for 6 h at 30 °C until it gives a white suspension. After reaction, the suspension was centrifuged and washed with water and ethanol by two cycles to remove any residual organics and ammonia. The final particles were collected after drying over-night at 80 °C then calcined at 500 °C for 5 h in static air (heating rate 2 °C min⁻¹).

2.1.1. Synthesis of V₂O₅/mesoporous silica spheres:

To prepare V₂O₅/MSS, the dried sample of mesoporous silica sphere (MSS) was impregnated with an aqueous solution of NH₄VO₃ that dissolved in oxalic acid solution and stirred at ambient temperature for 10 h. The obtained sample was first dried for 24 h at 120 °C and then calcined for 5 h at 550 °C in static air (heating rate 2 °C min⁻¹).

2.3. Characterization of the prepared sample:

X-ray diffractometer (XRD) (X'Pert PRO, Analytical, Netherlands) tested the crystal structure of the prepared samples using CuK α radiation at 40 kV, 2 θ = 0.02 ° phase size and 0.4 sec step time of scanning. N₂ adsorption-desorption isotherms (BET) estimated at liquid N₂ (-196 °C) by using a NOVA2000 gas sorption analyzer (Quanta Chrome Corporation) device was examined the texture properties. Fourier-transform infrared

spectroscopy (FT-IR) spectrum was reported between 500 and 4000 cm^{-1} with Perkin Elmer FTIR spectrometer (model one FT-IR spectrometer, USA). High-resolution transmission electron microscopy (HRTEM) was conducted by using a JEOL 2100F TEM at 200 kV of the accelerating voltage. To prepare TEM sample, A dilute colloidal sample mixture was ultra-sonicated in ethanol for 30 minutes and a drop of this solution was placed on a carbon-coated Cu TEM grid. The average particle size distribution of prepared samples was obtained by Dynamic light scattering (DLS). Analysis was carried out using measurements at 25 °C using a Zetasizer NanoZS (Malvern Instruments Ltd., UK).

2.4. Activity test:

The dual oxidation-adsorption efficiency of the $\text{V}_2\text{O}_5/\text{MSS}$ was examined for DBT removal from liquid fuels. In a standard experiment, a condenser, a thermometer, a magnetic bar and a hot plate were fitted with a 25 ml three-necked flask. In this flask, 0.02 g V_2O_5 / MSS and 0.4 ml H_2O_2 are applied to a definite concentration of 10 ml of DBT solution (in hexane as a solvent).

Different parameters that influence the efficiency of DBT removal have been investigated, such as the absence of adsorbent or an oxidizing agent, contact time (up to 300 minutes), reaction temperature (30-80°C) and initial DBT concentration (200-1000 mg L^{-1}). Also, the effect of stirring versus ultra-sonication on the removal efficiency was investigated. GC-FPD has been used to detect the concentration of residual DBT. The efficiency of DBT removal (%E) and the adsorption capacity q_e (mg g^{-1}) were determined as follows:

$$\% E = \frac{C_o - C_e}{C_o} * 100 \quad (1)$$

$$q_e = (C_o - C_e) \frac{V}{m} \quad (2)$$

Where C_o is the initial DBT concentration of its solution and C_e are remaining concentration of DBT after the adsorption (mg L^{-1}). V is the DBT volume in the solution, and m is the mass of the $\text{V}_2\text{O}_5/\text{MSS}$ (g).

3. RESULTS AND DISCUSSION

3-1 Characterization of the Prepared Samples:

XRD pattern of the prepared $\text{V}_2\text{O}_5/\text{MSS}$ after thermal treatment at 550°C in air is shown in Fig. 1. showed a broad diffraction peak in the region of 2θ 20-38° indicating that the silica samples are of amorphous structure matrix (1,33). Despite the amount of V_2O_5 , some low-intensity diffraction peaks related to the V_2O_5 supported on the amorphous silica pattern are observed (34).

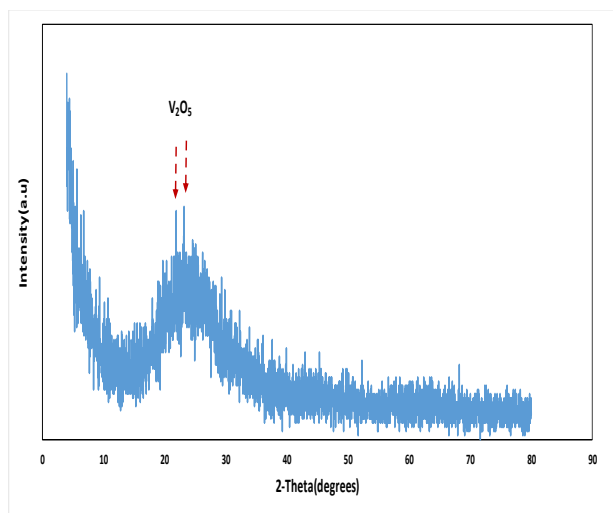


Fig. 1. XRD pattern of the prepared V_2O_5/MSS

Fig. 2. showed the FT-IR spectrum of the obtained samples at different preparation steps, dried core-shell solid silica spheres (SSCS), Mesoporous silica sphere (MSS) and V_2O_5/MSS . A distinctive Si-OH stretching vibration was displayed at about 3423 cm^{-1} . The structural differences between obtained (SSCS) and (MSS) were observed through the transverse optical mode of Si—O—Si asymmetric stretching vibration band exhibits a distinct red shift from 1101 to 1086 cm^{-1} of (MSS). The redshift of the Si—O—Si band suggests a more open structure in (MSS), which demonstrates the higher degree of condensation of silicate species (35). Also, The peaks at 2925 cm^{-1} and 2854 cm^{-1} were attributed to asymmetrical stretching vibration of -CH₃ and -CH₂-, which caused by organic matter inside the dried core-shell silica sample (SSCS) (36). The strong absorption peak at 1082 cm^{-1} was belonged to Si-O-Si asymmetric stretching(35). The peaks at 801 cm^{-1} and 464 cm^{-1} were assigned to symmetric stretching vibration of Si-O, and the peak at 964 cm^{-1} was due to bending vibration absorption of Si-OH. Peak around 1635 cm^{-1} was the bending vibration peak of H-O-H in water (36). The structural differences between obtained (MSS) and V_2O_5/MSS were observed where V_2O_5/MSS spectrum shows that the transverse. The peaks at 939 , 804 and 469 cm^{-1} belong to stretching vibration of terminal oxygen bonds of Si-O-V vibrations (37), the vibration of doubly coordinated oxygen (bridge oxygen) bonds, and the asymmetric and symmetric stretching vibration of triply coordinated oxygen (chain oxygen) bonds, respectively (38).

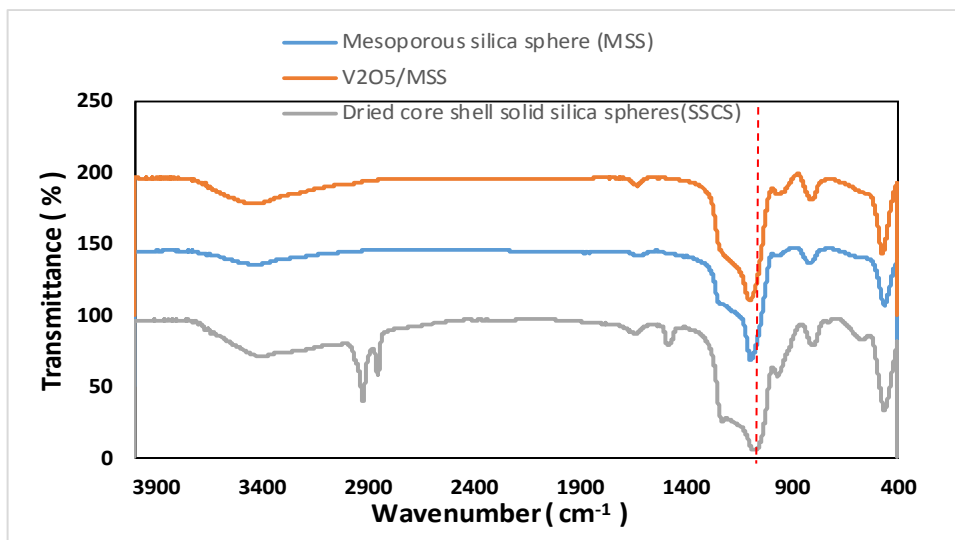


Fig. 2. FT-IR spectrum of the obtained samples at different preparation steps, Dried core shell solid silica spheres(SSCS), Mesoporous silica sphere (MSS), V₂O₅/MSS

HR-TEM images show the shape of the as-prepared samples. Typical show that as-prepared of dried core-shell solid silica spheres(SSCS) and Mesoporous Silica Sphere (MSS) after calcination are of spherical morphology (Fig. 3a, b), and SSCS exhibit a smooth surface while MSS show rough pore-like channels indicating the presence of micelle aggregates (35). The average radius of the spheres was not affected by calcination processes (PSD ~ 100 nm), as confirmed by DLS data (Fig. 3c).

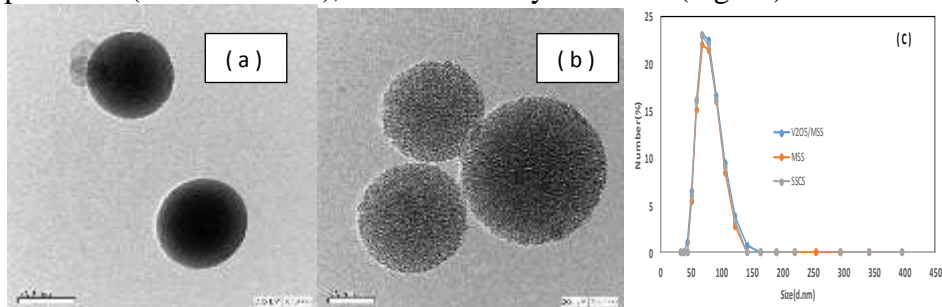


Fig . 3. HRTEM images of obtained samples at different preparation steps, (a) TEM image of as-prepared dried core-shell solid silica spheres(SSCS). (b) TEM of Mesoporous Silica Sphere (MSS) after calcination (c) Particle size distribution of Silica Sphere at different preparation steps and (V₂O₅/MSS) after calcination

Textural properties of the prepared V_2O_5/MSS samples are illustrated in (Fig. 4) Nitrogen adsorption-desorption shows type IV of isotherms, which are typical of mesoporous materials. The hysteresis loop of these isotherms can be classified as type H_3 , characterized by a triangular shape (39). Since the absorption and desorption branches appear at a relatively low pressure of about 0.4, materials with this kind of loop can be identified as materials with relatively uniform channel like-pores (40). Likewise, the pore diameter distribution determined with BJH method showed a broad range of pore diameters, mostly below 4 nm for samples synthesized. In the case of spherical, solid silica particles, specific surface areas as high as $403.501\text{m}^2/\text{g}$ correspond to diameters of 3.33 nm and total pore volume $0.5436\text{cm}^3\text{g}^{-1}$ which indicates the high porosity of the prepared sample (1,41)

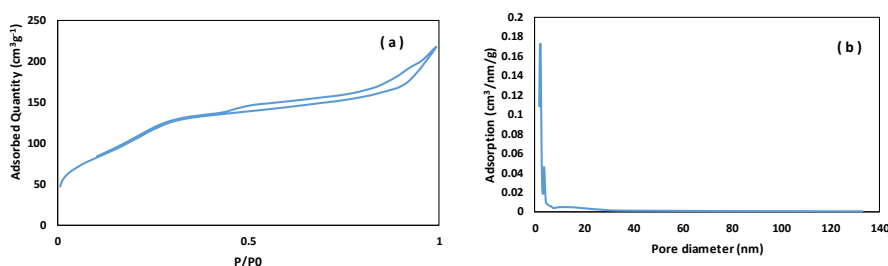


Fig. 4. N₂ adsorption-desorption isotherms (a), the corresponding pore size distribution plots obtained by BJH method (b)

3.2. Oxidative/Adsorptive Desulfurization Process

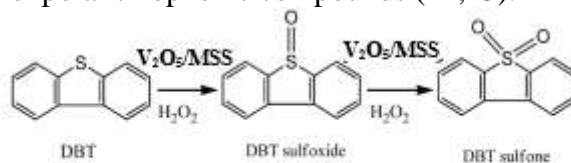
The dual oxidative/adsorptive desulfurization of DBT was tested by using the prepared catalyst V_2O_5/MSS . The desulfurization process was carried by using either stirring system or ultrasonicator as batch reaction systems in presence of an oxidizing agent as H_2O_2 . The model diesel fuel was prepared by dissolving DBT in n-hexane. Moreover, the dual oxidation-adsorption experiments were performed by changing temperature (30-70°C), initial concentration of DBT (200-1000 ppm) and the time from 10 to 300 min. To prove the coupling of catalytic oxidation and the adsorption process of prepared catalyst, the experiment was alternately carried out in the absence and presence of the V_2O_5/MSS or H_2O . First of all, the desulfurization process was carried on 600 ppm of DBT for 60 min under stirring system at 60°C, in the absence and presence of 0.02 g V_2O_5/MSS and/or 0.4 ml of H_2O_2 . The removal efficiency (%E) was detected and presented in (Table. 1). From the obtained result, It is obvious that Using V_2O_5/MSS without the oxidizing agent showed low removal efficiency (%E) which prove the low adsorptive ability of V_2O_5/MSS toward DBT. However, using of H_2O_2 in absence of V_2O_5/MSS results in poor removal

(%E), which indicates the slow rate of DBT oxidation. Using both V_2O_5/MSS and H_2O_2 enhances significantly the removal (%E) which indicates the dual oxidative adsorption property of the prepared catalyst.

Table 1. Removal (%E) of DBT in presence and absence of V_2O_5/MSS

Experiment no.	V_2O_5/MSS (g)	H_2O_2 (ml)	(%E)
			60 °C
1	0.02	-	39.34
2	-	0.4	27.61
3	0.02	0.4	71.5

This data indicates the oxidative ability of the prepared catalyst V_2O_5/MSS of DBT by H_2O_2 producing sulfones and/or sulfoxides forms (scheme. 1). In consequence, The adsorption capacity increases due to the greater adsorptive affinity toward sulfoxides and sulfones (polar $O=S=O$) than nonpolar thiophenic compounds (42,43).



Scheme. 1. Catalytic Oxidative desulfurization of DBT to DBT sulfone

3.2.2. Effect of contact time

In order to find a suitable equilibrium contact time, this test was carried out at time intervals ranging from 10 to 300 min. the removal (%E) of model diesel of DBT using oxidative/adsorptive system as a function of interval contact time at 60 °C shown by Fig. 5 comparing both stirring and sonication techniques. At either stirring or sonication, the removal (%E) increases by increasing the reaction time till equilibrium that's due to the availability of vacant active sites on V_2O_5/MSS surface. then the oxidative desulfurization process to sulphone slows down due to occupying the active sites. Hence, In the case of stirring, 120 min was selected for further experiments. Comparing these results with the previous work indicates that, V_2O_5/MSS dual system achieved to equilibrium faster than those based only on adsorption (44,45), but the desulfurization process attained equilibrium 90 min in the case of sonication. This can be recognized by the specific effect of ultrasound waves, where micro-streaming bubbles are produced by the acoustic cavitation of the ultrasonic technique, which improves mass transfer in the reaction mixture (46,47).

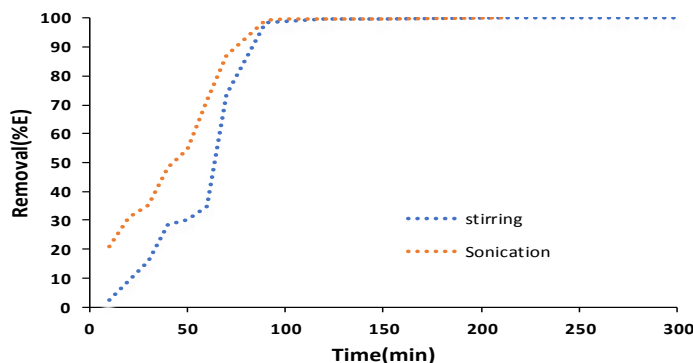


Fig. 5. Effect of contact time (% E) under stirring or sonication on 0.02 g of adsorbent, 10 ml of 600 ppm DBT solution for 300 min

Adsorption kinetics study

Kinetics of The experimental results have been studied by applying the well-known pseudo-first-order and pseudo-second-order models (48,49). Their expressions of mathematics are given in Eqs. (3 – 5).

The pseudo-first-order model is written as follows:

$$\ln (q_e - q_t) = \ln q_e - k_1 t \tag{3}$$

The pseudo second order equation is stated as follows:

$$\frac{t}{q_t} = \frac{1}{k_2 q_e^2} + \frac{t}{q_e} \tag{4}$$

$$R_t = k_2 q_e^2 \tag{5}$$

where q_e and q_t are the adsorbed amounts at equilibrium (mg g^{-1}) and time t respectively while k_1 (min^{-1}) is the rate constant of pseudo first-order adsorption that calculated from linear plot of $\text{Log} (q_e - q_t)$ versus time. k_2 ($\text{g.mg}^{-1} \text{min}^{-1}$) is the rate constant of pseudo second order adsorption which can calculated by Plotting a straight line from t/q_t verses t . the value of the correlation coefficient (R^2) was used to choose the best-fit model. Table. 2 and (Fig. 6) showed a better fitting to pseudo- first-order model with $R^2 \approx 1$ under sonication or stirring. Also, it shows the comparable theoretical values q_e with to the experimental values.

Table. 2. Detected kinetics parameters for dual oxidative adsorption of DBT (600 mg/l); 120 min at 60°C

Conditions	experimental q_e (mg/g)	pseudo- first order			pseudo- second order		
		q_e (mg/g)	$K_1 \times 10^3$ (min^{-1})	R^2	q_e (mg/g)	$K_2 \times 10^3$ ($\text{g.mg}^{-1}.\text{min}^{-1}$)	R^2
Stirring	299.288	317.770	0.008	0.970	-78.457	0.14	0.573
Sonication	299.585	309.318	0.019	0.912	404.172	0.037	0.701

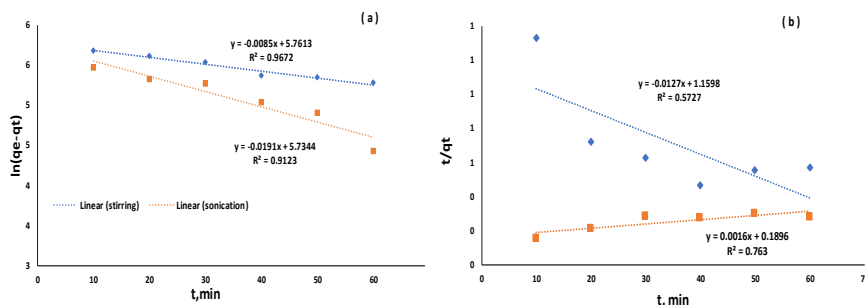


Fig. 6. Models of Kinetic for the adsorption process (a) pseudo first-order kinetic model, (b) pseudo-second-order model.

3.2.3. Effect of initial concentration

To find the maximum capacity of V_2O_5/MSS as adsorbent, five samples of DBT solution with different concentrations of 200, 400, 600, 800, and 1000 ppm were used. This parameter was carried by using 0.02g of V_2O_5/MSS dual system for 120 min at 60°C under stirring. As shown fig. 7 the amounts adsorbed (mg g^{-1}) increases with increasing of initial concentration that's due to improve the mass transfer of adsorbate species from the bulk solution to the adsorbent surface (44,45,50). Additionally, the sample did not achieve saturation up to initial concentration of 1000 mg L^{-1} .

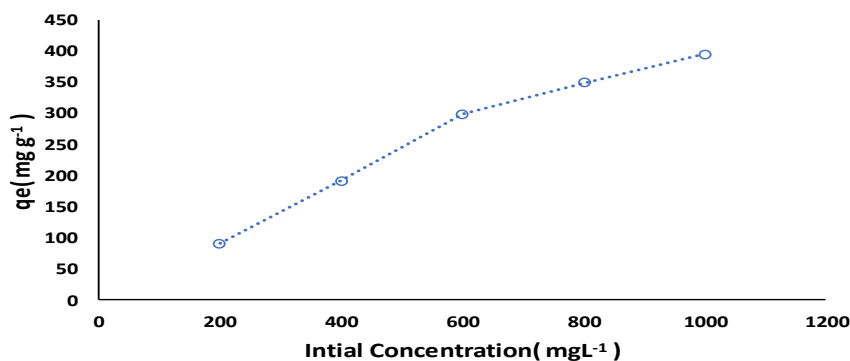


Fig. 7. Adsorption capacity as function of DBT initial concentration at 60°C under stirring on 0.02 g of adsorbent, 10 ml of 600 ppm DBT solution for 120 min

3.4. Adsorption isotherm

Models of adsorption isotherms were also used to study the Adsorption process at equilibrium as a function of initial DBT concentration. Two models Langmuir and Freundlich.

The Langmuir isotherm (51) can be expressed mathematically as the following Eq (6).

$$\frac{C_e}{q_e} = \frac{1}{bQ_e} + \frac{C_e}{Q_e} \tag{6}$$

Where C_e is the equilibrium concentration of DBT in solution (mg/L), Q_e is the maximum theoretical capacity at the monolayer (mg/g) and b is the constant of Langmuir (l/mg).

The Freundlich isotherm (52) can be expressed mathematically as the following Eq (7).

$$\log q_e = \log k_f + \frac{1}{n} \log C_e \tag{7}$$

where q_e (mg/g) is the DBT amount adsorbed at equilibrium, C_e (mg/L) is the remaining concentration of DBT in model oil, K_F the Freundlich constant [$\text{mg/g} (\text{mg/l})^n$] represents adsorption capacity and n is adsorption favorability constant which they are calculated from slope and intercepts of linear plot of $\ln q_e$ against $\ln C_e$. The value of $1/n$ is being closer to 0, which implies that the adsorbent surface is more heterogeneous and promotes the multilayer adsorption process.

Table. 3. and (Fig. 8) showed the calculated values of models. The model of Langmuir isotherm has a good fittings of the experimental data with $R^2 = 0.909$ which suggests a monolayer adsorption process on the homogeneous surface of the adsorbent.

Table. 3. Obtained data from fitting experimental results with the three models:

Langmuir	$b(\text{L mg}^{-1})$	0.031556578
	$q_{\max}(\text{mg g}^{-1})$	450.6500415
	R^2	0.909470584
Freundlich	$K_f((\text{mg/g})/(\text{mg/L})^n)$	177.4819303
	$1/n$	0.08724925
	R^2	0.078955289

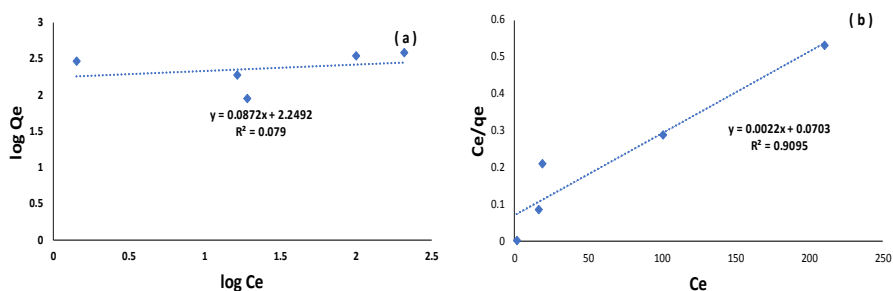


Fig. 8. The dual oxidative adsorption models for DBT removal : (a) Langmuir isotherm, and (b) Freundlich isotherm.

3.5. Adsorption mechanism

It is known that the adsorption mechanism follows a complex pathway and is followed by both the surface and the diffusion of the pore but in different areas. The intra_particle diffusion model was evaluated according to “Weber and Morris equation” to investigate the diffusion process (53,54).

The initial rate of intra-particle diffusion in this model can be expressed mathematically as the following equation:

$$q_t = k_i t^{1/2} + C \quad (8)$$

where k_i is the constant of the intra_particle diffusion rate ($\text{mg/g}\cdot\text{min}^{0.5}$), and C (mg/g) is a constant attributed to the boundary layer effect and obtained from the intercept value by plotting q_t versus ($t^{0.5}$). In this equation, the C value give a picture about the rate-determining step where, $C = 0$, intraparticle diffusion is the only rate-determining step and $C \neq 0$, the process was controlled by a variety of mechanism

As shown in (Fig. 9), the multilinear relationship with $C > 0$, indicate that, more than one step occurred during the desulfurization process over the prepared catalyst adsorbent ($\text{V}_2\text{O}_5@\text{MSS}$) system under both stirring and ultrasonication. This implies that adsorption takes place in three stages; the early stage is the rapid adsorption of the surface, followed by the slower stage of intra-particle diffusion and finally the equilibrium stage (46,47).

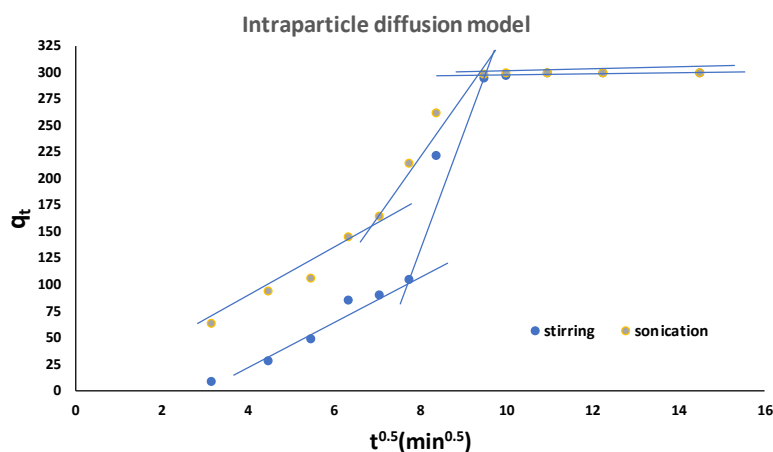


Fig. 9. Intra-particle diffusion plot for adsorption of 600 mg/l of as initial concentration of DBT at 60°C for 120 min

3.6. Thermodynamics studies

The key factor for both catalytic and adsorptive desulfurization reactions is temperature (55). The influence of temperature was set on the DBT solution desulfurization process using V_2O_5 / MSS as a dual catalyst-adsorbent system has been investigated. The adsorption process was performed at various temperatures under stirring (303, 313, 323, 333 and 343 K). (Fig. 10) displays the relation between adsorption capacity (q_e) and temperature. It shows that a gradual increase in removal (percent E) was obtained by increasing the temperature applied from 303 to 333 K and improving the dual oxidative / adsorption process. However, a further rise in the temperatures of reaction leads to a reduction in the potential of adsorption. This has been shown by the decomposition of H_2O_2 into water, which reduces sulfone production (43). These results indicate that the process of desulfurization using V_2O_5 / MSS occurs adequately at temperatures equal to or even lower than 333 K (56).

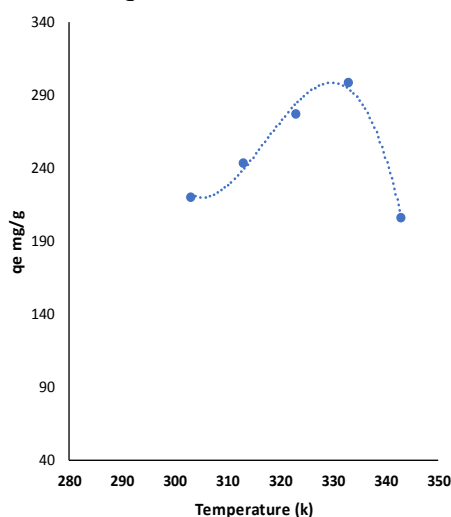


Fig. 10. The adsorption capacity as a function of applied temperature using V_2O_5 /MSS under stirring; 600 ppm of DBT as initial concentration at 60°C for 120 min.

The thermodynamic adsorption parameters as change of free Gibbs energy (ΔG), change of enthalpy (ΔH) (kJ mol^{-1}) and change of entropy (ΔS) ($\text{J mol}^{-1} \text{K}^{-1}$) were determined by using the results of experimental adsorption isotherms up to 333 K. The thermodynamic adsorption parameters (ΔH), (ΔG) and (ΔS) were calculated by using the following equations (9-11):

$$K_d = \frac{q_e}{C_e} \quad (9)$$

$$\Delta G = -RT \ln K_d \quad (10)$$

$$\ln K_d = \frac{\Delta S}{R} - \frac{\Delta H}{RT} \quad (11)$$

where R ($8.314 \times 10^{-3} \text{ kJ K}^{-1} \text{ mol}^{-1}$) is the gas constant and T is the applied kelvin temperature (K). from (Eq. 13), ΔG was demonstrated while from slope and intercept from the plot of $\ln K_d$ versus $1/T$ of (Eq. 14), (ΔH) and (ΔS) were measured. The values of ΔH and ΔS are presented in (Table. 4) (ΔS) and (ΔH) showed positive values that suggest that the adsorption mechanism of endothermic catalytic oxidation contributes to a growing disorder. (ΔS) and (ΔH) show positive values and hence the negative sign of (ΔG) indicates the spontaneity of adsorption process (54,57,58).

It showed positive values

Table. 4. Thermodynamic parameters for dual oxidation adsorption process of DBT (600 mg g^{-1}) for 120 min under stirring.

T (K)	$\ln K_d$	$\Delta G \text{ (KJ mol}^{-1}\text{)}$	$\Delta H \text{ (KJ mol}^{-1}\text{)}$	$\Delta S \text{ (J mol}^{-1} \text{ K}^{-1}\text{)}$
303	0.332362832	-0.837269169		
313	0.778222795	-2.02515517	37.57273881	130.4431184
323	1.807364104	-4.853535328		
333	5.347294101	-14.80431525		

CONCLUSION

In conclusion, our study successfully synthesized mesoporous silica spheres via micelle-template and V_2O_5 nano-particles supported on it (V_2O_5 /MSS) through impregnation technique. This novel catalyst proved its effect as a novel dual oxidative/adsorptive system of model diesel fuel. The Desulfurization process is performed in the presence a suitable oxidizing agent (H_2O_2) at different conditions of temperature, contact time and initial concentration under either stirring or ultrasonication. The novel catalyst shows an effective removal about 100 % under sonication within 1.5h but in stirring within 2h. The pseudo-first - order model could explain adsorption kinetics (V_2O_5 / MSS) of the studied adsorbents. The experimental data matches well with the Langmuir model of the isotherm which indicates a monolayer adsorption process on the homogeneous surface of the adsorbent. The determined thermodynamic parameters suggested that the endothermic adsorption process was favorable for (V_2O_5 / MSS) adsorption.

Declaration of Competing Interest

The authors declare that they have no known competing financial interests or personal relationships that could have appeared to influence the work reported in this paper.

Acknowledgment

The authors acknowledge the financial support from the Academy of Scientific Research and Technology in Egypt to the scientific research students through the program of Next Generation Scholars. (ASRT- SNG 5-2016).

REFERENCES:

1. **Zhu, K. ; Y. Du ; X. Wu ; X. You ; Y. He ; Y. Qu ; Z Jing and Z. Shan (2020):** Fast Synthesis of uniform mesoporous silica spheres. *Materials Letters.*; 273:127947.
2. **Schmidt, H.K. ; E. Geiter ; M. Mennig ; H. Krug ; C. Becker and R.P.Winkler (1998):** The Sol-Gel Process for Nano-Technologies: New Nanocomposites with Interesting Optical and Mechanical Properties. *Journal of Sol-Gel Science and Technology.*;13(1-3):397-404.
3. **Fu, Z. ; G. Zhang ; Z. Tang and H. Zhang (2020):** Preparation and Application of Ordered Mesoporous Metal Oxide Catalytic Materials. Vol. 24, *Catalysis Surveys from Asia.*, p. 38-58.
4. **de Greñu, B.D. ; R. de los Reyes ; A.M. Costero ; P. Amorós and J.V. Ros-Lis (2020):** Recent progress of microwave-assisted Synthesis of silica materials. Vol. 10, *Nanomaterials.* MDPI AG.
5. **Kumar, S. ; M.M. Malik and R. Purohit (2017):** Synthesis Methods of Mesoporous Silica Materials. *Materials Today: Proceedings.*;4(2):350-357.
6. **El-toni, A.M. ; M.A. Habila ; P. Labis ; J.P. Labis ; Z.A. Alothman ; M. Alhoshan ; A.A. Elzatahry and F. Zhangg (2016):** Design, Synthesis and applications of core-shell, hollow core, and nanorattle multifunctional nanostructures. *Nanoscale.*; 8(5): 2510-2531.
7. **Li, X.H. ; Y.X. Zhang ; Z.L. Liu ; Q.Z. Liu ; B. Li ; G.P. Zhu and K. Dai (2014):** A facile and novel approach for preparing monodispersed hollow aluminosilica microspheres with thin shell structures. *RSC Advances.*;4(107):62209-62214.
8. **Jankiewicz, B.J. ; D. Jamiola ; J. Choma and M. Jaroniec (2012):** Silica-metal core-shell nanostructures. *Advances in Colloid and Interface Science.*;170(1-2):28-47.
9. **Liu, J. ; S.Z. Qiao ; Q.H. Hu and G.Q. Lu (2011):** Magnetic nanocomposites with mesoporous structures: Synthesis and applications. *Small.* 2011;7(4):425-43.
10. **Priebe, M. and K.M. Fromm (2014):** Nanorattles or yolk-shell nanoparticles-what are they, how are they made, and what are they good for? *Chemistry - A European Journal.*;21(10):3854-3874.
11. **Yang, T. ; R. Zhou ; D.W. Wang ; S.P. Jiang ; Y.Yamauchi ; S.Z. Qiao ; M.J. Monteiro and J. Liu (2015):** Hierarchical

- mesoporous yolk-shell structured carbonaceous nanospheres for high performance electrochemical capacitive energy storage. *Chemical Communications*.;51(13):2518–2521.
12. **Liu, M. ; B.Su ; Y. Tang ; X. Jiang and A.Yu (2017):** Recent advances in nanostructured vanadium oxides and composites for energy conversion. *Advanced Energy Materials*.;7(23):1–34.
 13. **Arellano, U. ; Z. Wang ; L. Chen ; J.A. Wang ; M. Asomoza and A. Estrella (2017):** VOx Core-Shell Catalysts for One-Pot Oxidation and Separation of Refractory Multiaromatic Sulfur Compounds in a Model Diesel. *Industrial and Engineering Chemistry Research*.;56(42):12080–12091.
 14. **Nanoti, A. ; S. ; Dasgupta ; A.N. Goswami ; B.R. Nautiyal ; T.V. Rao ; B. Sain ; Y.K. Sharma ; S.M. Nanoti ; M.O. Garg and P. Gupta (2009):** Mesoporous silica as selective sorbents for removal of sulfones from oxidized diesel fuel. *Microporous and Mesoporous Materials*.;124(1–3):94–99.
 15. **Safa, M.A. ; R. Al-Majren ; T. Al-Shamary ; J. Park and X. Ma (2017):** Removal of sulfone compounds formed in oxidative desulfurization of middle distillate. *Fuel*.;194:123–128.
 16. **Han, Y. ; Y. Zhang ; C. Xu and C.S. Hsu (2018):** Molecular characterization of sulfur-containing compounds in petroleum. *Fuel*.;221:144–158.
 17. **Tavan, Y. ; M. Shahrokhi and F. Farhadi (2020):** Electrochemical oxidative desulfurization for high sulfur content crude gas-oil. *Separation and Purification Technology*.;248:117117.
 18. **Campos-Martin, J.M. ; M.C. Capel-Sanchez ; P. Perez-Presas and J.L.G. Fierro (2010):** Oxidative processes of desulfurization of liquid fuels. *Journal of Chemical Technology and Biotechnology*.;85(7):879–890.
 19. **Ishihara, A. ; D. Wang ; F. Dumeignil ; H. Amano ; E.W. Qian and T. Kabe (2005):** Oxidative desulfurization and denitrogenation of a light gas oil using an oxidation/adsorption continuous flow process. *Applied Catalysis A: General*.;279(1–2):279–287.
 20. **Gates, B.C. and H. Topsøe (1997):** Reactivities in deep catalytic hydrodesulfurization: Challenges, opportunities, and the importance of 4-methyldibenzothiophene and 4,6-dimethyldibenzothiophene. *Polyhedron*.;16(18):3213–3217.
 21. **Wang, Q. ; T. Zhang ; S. Zhang ; Y. Fan and B. Chen (2020):** Extractive desulfurization of fuels using trialkylamine-based protic ionic liquids. *Separation and Purification Technology*.;231:115923.
 22. **Kareem, Y.S. ; S.H. Ammar and R.A. Darwash (2020):**

- Microwave-induced catalytic oxidative desulfurization of gasoil fraction over phosphotungstic acid-based magnetic silica (Ni @ SiO₂ \ PWA) nanocatalyst. Catalysis Communications.;136:105926.
23. **Dana, M. ; M.A. Sobati ; S. Shahhosseini and A. Rahbar-Kelishami (2019):** Separation of sulfur-containing compounds from diesel by oxidation followed by solvent extraction in a single drop column. Brazilian Journal of Chemical Engineering.;36(3):1343–1355.
 24. **Sinhmar, P.S. and P.R. Gogate (2020):** Ultra-deep desulfurization of crude sulfated turpentine using oxidation, adsorption and novel combination approach. Environmental Technology and Innovation.;18:100682.
 25. **Guo, T. ; W. Jiang ; Y. Ruan ; L. Dong ; H. Liu ; H. Li ; W. Zhu and H. Li (2018):** Superparamagnetic Mo-containing core-shell microspheres for catalytic oxidative desulfurization of fuel. Colloids and Surfaces A: Physicochemical and Engineering Aspects.; 537: 243–249.
 26. **Mojaverian, K.A. ; A. Ahmadpour ; B.T. Rohani and M. Ghahramaninezhad (2018):** Deep oxidative desulfurization of dibenzothiophene with {Mo132} nanoballs supported on activated carbon as an efficient catalyst at room temperature. New Journal of Chemistry.;42(14):12188–12197.
 27. **Shi, Y. ; G.Liu and X. Zhang (2017):** Adsorptive Removal of Dibenzothiophene and Dibenzothiophene Sulfone over Mesoporous Materials. Industrial and Engineering Chemistry Research.; 56(9):2557–2564.
 28. **Samaniego, M.L. ; M.D.G. De Luna ; D.C. Ong ; M.W. Wan and M.C. Lu (2019):** Isotherm and Thermodynamic Studies on the Removal of Sulfur from Diesel Fuel by Mixing-Assisted Oxidative-Adsorptive Desulfurization Technology. Energy and Fuels.;33(2):1098–1105.
 29. **Shi, Y. ; G. Liu and X. Zhang (2017):** Adsorptive Removal of Dibenzothiophene and Dibenzothiophene Sulfone over Mesoporous Materials. Industrial and Engineering Chemistry Research.;56(9):2557–2564.
 30. **Sinhmar, P.S. and P.R. Gogate (2020):** Ultrasound assisted oxidative desulfurization of simulated diesel using flow cell and longitudinal bath in combination with different oxidants. Chemical Engineering and Processing - Process Intensification.;153:107968.
 31. **Abdi, G. ; M. Ashokkumar and A. Alizadeh (2017):** Ultrasound-assisted oxidative-adsorptive desulfurization using highly acidic graphene oxide as a catalyst-adsorbent. Fuel.; 210: 639–645.
 32. **Ban, L. ; P. Liu ; C. Ma and B. Dai (2013):** Deep

- oxidative/adsorptive desulfurization of model diesel oil by DBD/FeCl₃-SiO₂. *Catalysis Today*.;211:78–83.
33. **Wang, H. ; L. Peng ; Z. Huang and S. Mei (2014):** Well-dispersed hollow silica microspheres synthesis with silica sol as precursor by template method. *Journal of Molecular Structure*.;1059(1):15–19.
 34. **Farzaneh, F. ; E. Zamanifar ; L. Jafari Foruzin and M. Ghandi (2012):** Synthesis and characterization of V₂O₅/SiO₂ nanoparticles as efficient catalyst for aromatization 1,4 dihydropyridines. *Journal of Sciences, Islamic Republic of Iran*.;23(4):313–318.
 35. **Chen, Y. ; H. Chen ; L. Guo ; Q. He ; F. Chen ; J. Zhou ; J. Feng and J. Shi (2010):** Hollow/rattle-type mesoporous nanostructures by a structural difference-based selective etching strategy. *ACS Nano*.;4(1):529–539.
 36. **Bao, Y. ; T.Wang ; Q. Kang ; C. Shi and J. Ma (2017):** Micelle-template synthesis of hollow silica spheres for improving water vapor permeability of waterborne polyurethane membrane. *Scientific Reports*.;7:1–14.
 37. **Agger, J.R. ; M.W. Anderson ; M.E. Pemble ; O. Terasaki and Y. Nozue (1998):** Growth of quantum-confined indium phosphide inside MCM-41. *Journal of Physical Chemistry B*.;102(18):3345–3353.
 38. **Zhang, J. ; X. Bai ; X. Li ; A. Wang and X. Ma (2009):** Preparation of MoO₃-CeO₂-SiO₂ oxidative desulfurization catalysts by a sol-gel procedure. *Cuihua Xuebao/Chinese Journal of Catalysis*.;30(10):1017–1021.
 39. **Illescas, J.F. and M.J. Mosquera (2012):** Producing surfactant-synthesized nanomaterials in situ on a building substrate, without volatile organic compounds. *ACS Applied Materials and Interfaces*.;4(8):4259–4269.
 40. **Wang, M. ; Q. Zeng ; B. Zhao and D. He (2013):** Application of tailored silica microspheres in coatings: Synthesis, characterization, thermal and hydrophobic properties. *Journal of Materials Chemistry A*.;1(37):11465–11472.
 41. **Ijaz, A. ; M.B. Yagci ; C.W. Ow-Yang ; A.L. Demirel and A. Mikó (2020):** Formation of mesoporous silica particles with hierarchical morphology. *Microporous and Mesoporous Materials*. 2020;303(April).
 42. **Ma, X. ; A. Zhou and C.Song (2007):** A novel method for oxidative desulfurization of liquid hydrocarbon fuels based on catalytic oxidation using molecular oxygen coupled with selective adsorption. *Catalysis Today*.;123(1–4):276–84.

43. **Teimouri, A. ; M. Mahmoudsalehi and H. Salavati (2018):** Catalytic oxidative desulfurization of dibenzothiophene utilizing molybdenum and vanadium oxides supported on MCM-41. *International Journal of Hydrogen Energy*.;43(31):14816–14833.
44. **Radwan, D.R. ; A. Matloob ; S. Mikhail ; L. Saad and D. Guirguis (2019):** Metal organic framework-graphene nanocomposites for high adsorption removal of DBT as hazard material in liquid fuel. *Journal of Hazardous Materials*.;373:447–458.
45. **Yang, K. ; Y. Yan ; W. Chen ; H. Kang ; Y. Han ; W. Zhang ; Y. Fan and Z. Li (2018):** The high performance and mechanism of metal–organic frameworks and their composites in adsorptive desulfurization. *Polyhedron*.;152:202–215.
46. **Kuppa, R. and V.S. Moholkar (2010):** Physical features of ultrasound-enhanced heterogeneous permanganate oxidation. *Ultrasonics Sonochemistry*.;17(1):123–31.
47. **Abdi, G. ; M. Ashokkumar and A. Alizadeh (2017):** Ultrasound-assisted oxidative-adsorptive desulfurization using highly acidic graphene oxide as a catalyst-adsorbent. *Fuel*.;210:639–645.
48. **Ho, Y.S. and G.A. McKay (1998):** Comparison of chemisorption kinetic models applied to pollutant removal on various sorbents. *Process Safety and Environmental Protection*.;76(4):332–40.
49. **Abou-Gamra, Z.M. and M.A. Ahmed (2015):** TiO₂ Nanoparticles for Removal of Malachite Green Dye from Waste Water. *Advances in Chemical Engineering and Science*.;05(03):373–388.
50. **Ullah, S. ; S. Hussain ; W. Ahmad ; H. Khan ; K.I. Khan ; S.U. Khan and S. Khan (2020):** Desulfurization of Model Oil through Adsorption over Activated Charcoal and Bentonite Clay Composites. *Chemical Engineering and Technology*., 43(3):564–73.
51. **Foo, K.Y. and B.H. Hameed (2010):** Insights into the modeling of adsorption isotherm systems. *Chemical Engineering Journal*.;156(1):2–10.
52. **Freundlich, H. (1907):** Über die adsorption in lösungen. *Zeitschrift für physikalische Chemie*.;57(1):385–470.
53. **Cheung, W.H. ; Y.S. Szeto and G. McKay (2007):** Intraparticle diffusion processes during acid dye adsorption onto chitosan. *Bioresource Technology*. 98(15):2897–2904.
54. **Omnia, A.L.I. and S. Mohamed (2017):** Adsorption of copper ions and alizarin red S from aqueous solutions onto a polymeric nanocomposite in single and binary systems. *Turkish Journal of Chemistry*.;41(6):967–86.
55. **Zaheer, K. and A. Syed (2015):** Oxidative desulphurization followed by catalytic adsorption method. *South African Journal of*

- Chemical Engineering.;18(2):14–28.
56. **Pan, Y. ; M. Chen ; M. Hu ; M. Tian ; Y. Zhang and D. Long (2020):** Probing the room-temperature oxidative desulfurization activity of three-dimensional alkaline graphene aerogel. Applied Catalysis B: Environmental.;262:118266.
57. **Gailey, W.K.D. and E. Raymond (1992):** General Chemistry, 4th Edition. Saunders College Publishing.69(7):1992.
58. **Ahmadi, M. ; M Mohammadian ; M.R. Khosravi-Nikou and A. Baghban (2019):** Experimental, kinetic, and thermodynamic studies of adsorptive desulfurization and denitrogenation of model fuels using novel mesoporous materials. Journal of Hazardous Materials., 15(374):129–139.

تحضير خامس اكسد الفانديم النانوي المحمل على كريات السليكا المسامية

(V₂O₅/MSS) لإزالة الكبريت بطريقة الأكسدة-الامتزازية الجديدة

شروق شوقي*¹، ناصر حلمي شلبي¹، داليا رضوان عبد الحافظ¹، سمر سعيد¹،

ماهر حلمي هلال²، سحر كمال محمد²

¹معمل الحفازات، قسم التكرير، معهد بحوث البترول المصرى، مدينة نصر، 11727، القاهرة

²قسم الكيمياء، كلية العلوم، جامعة حلوان، عين حلوان، حلوان، 11795، القاهرة، مصر

تم تحضير خامس اكسد الفانديم النانوي المحمل على كريات السليكا المسامية (V₂O₅/MSS) باستخدام تقنية التشريب impregnation. حيث تم تحضير كريات السليكا المسامية باستخدام micelle-template method. تم توصيف المادة المحضرة باستخدام تقنيات ال XRD و FTIR و BET و DLS. أظهرت النتائج أن العينات كانت غير متبلورة ومسامية الشكل، وذات مساحات داخلية خاصة، وكذلك مساحة سطح مميزة عالية. تم اختبار العينة المحضرة للأداء الأكسدة / الامتزاز oxidative/adsorptive لنموذج وقود الديزل. تم اختبار عملية إزالة الكبريت في وجود ال H₂O₂ كعامل مؤكسد تحت ظروف تفاعل مختلفة (درجة الحرارة ووقت التلامس والتركيز الأولي) باستخدام نظام المفاعل الثابت عن طريق التقليب أو في وجود الموجات فوق الصوتية. تشير البيانات إلى أن V₂O₅/MSS يظهر أداءً جيداً تجاه إزالة الكبريت المؤكسدة / الامتزازية مع كفاءة إزالة بنسبة 100٪ في حالة استخدام تقنية الموجات الصوتية خلال 1.5 ساعة. ولكن باستخدام تقنية التقليب وصلت نسبة الكفاءة إلى 100٪ خلال ساعتين عند 60 درجة مئوية باستخدام تركيز أولي 600 جزء في المليون. تتمثل الفائدة الاقتصادية لهذه الدراسة في إزالة الكبريت بكفاءة من خلال اقتران الأكسدة والامتزاز لثنائي بنزوثيوفين DBT في ظروف درجة الحرارة العادية دون الحاجة إلى مواد ماصة إضافية أو استخدام تقنيات الاستخراج.